

Insights into the Self-Filling Effects of Branched Isopropyl Groups on the Conformational and Supramolecular Properties of Isopropoxyprism[6]arene

Rocco Del Regno,^{*,[a]} Paolo Della Sala,^[a] Neal Hickey,^[b] Silvano Geremia,^{*,[b]} Carmen Talotta,^[a] Placido Neri,^[a] and Carmine Gaeta^{*,[a]}

This paper is dedicated to the memory of the late Prof. Wei Jiang, who made significant contributions to the development of naphthol-based supramolecular hosts

In this work, the direct macrocyclization of a prism[6]arene macrocycle bearing branched alkyl chains on the rims is reported. Isopropoxyprism[6]arene adopts in solution and in the solid state a cuboid D_2 -conformation in which four isopropyl groups are folded inside the cavity, to give C–H $\cdots\pi$ interactions and filling the internal void. The conformational features of isopropoxyprism[6]arene have been studied by dynamic ^1H NMR experiments. The presence of branched isopropyl chains

on the prism[6]arene rims, stabilizes the cuboid D_2 -conformation to a greater extent than ethyl or propyl groups in PrS[6]^{Et} and PrS[6]^{nPr}. The higher resistance of PrS[6]^{iPr} to open its cuboid D_2 conformation, with respect to PrS[6]^{Et} and PrS[6]^{nPr}, also affected its binding abilities. In fact, alkylammonium-based *endo*-cavity complexes of PrS[6]^{iPr} show lower binding constant values than the analogous propoxy/ethoxy-prism[6]arene complexes.

Introduction

In recent years macrocyclic hosts have played a significant role in supramolecular chemistry.^[1] The design of new macrocycles^[2] takes inspiration from natural biological receptors, which show deep binding sites that ensure large contact area and multiple interaction sites. Among natural receptors, enzymes show great binding efficiency and recognition selectivity.^[3] In biomimetic chemistry novel intriguing deep-cavity macrocycles have been developed based on naphthalene or anthracene monomers, such as, oxatubarenes,^[4] naphthotubes,^[5] pagoda[n]arene,^[6] calixnaphtharene,^[7] and naphthocages.^[8,9] Wei Jiang^[5] recently reported the naphthotubes, deep-cavity macrocycles with polar amido functions embedded inside the cavity and with the

ability to complex neutral guests in water by hydrophobic effect and H-bonding interactions.^[10,11] More recently we have reported a novel class of deep-cavity macrocycles named prismarenes PrS[n]^R and constituted by 1,5-methylene bridged 2,6-dialkoxynaphthalene units.^[12–17] Prismarenes show a π -electron rich aromatic cavity able to form *endo*-cavity complexes with alkylammonium guests stabilized by C–H $\cdots\pi$ and cation $\cdots\pi$ interactions.

Very recently,^[14] we showed that, differently from methoxy which show a preference for the formation of five membered macrocycles, ethoxy and propoxy prism[6]arene (Figure 1a) can be obtained in very high yields and short reaction times using different solvent, toluene, decaline, cyclohexane, chlorocyclohexane and 1,2-dichloroethane. Ethoxy and propoxy-

[a] Dr. R. Del Regno, Dr. P. Della Sala, Prof. C. Talotta, Prof. P. Neri, Prof. C. Gaeta
Laboratory of Supramolecular Chemistry
Department of Chemistry and Biology "A. Zambelli"
University of Salerno
Via Giovanni Paolo II 132
Fisciano, 84084 (Italy)
E-mail: rodelregno@unisa.it
cgaeta@unisa.it

[b] Dr. N. Hickey, Prof. S. Geremia
Centro di Eccellenza in Biocristallografia
Dipartimento di Scienze Chimiche e Farmaceutiche
Università di Trieste
via L. Giorgieri 1
34127 Trieste (Italy)
E-mail: sgeremia@units.it

Supporting information for this article is available on the WWW under <https://doi.org/10.1002/ejoc.202300608>

Special Collection Part of the "DCO-SCI Prize and Medal Winners 2022" Special Collection.

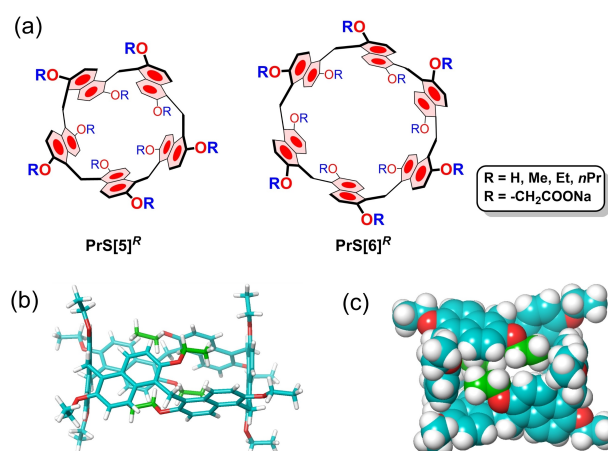


Figure 1. (a) Chemical drawing of Prism[n]arenes^[12–17]; (b and c) Different views of the solid state structure^[14] of PrS[6]^{Et}.

prism[6]arene in Figure 1, adopt, both in solution and in the solid state, a cuboid-shaped D_2 -conformation in which four alkyl chains fill the inner cavity of the macrocycle (Figure 1b and 1c). In the presence of appropriate alkylammonium guests the cuboid- D_2 -conformation of ethoxy and propoxy-prism[6]arene opens up to yield a more symmetrical D_6 -conformation^[14] able to host cationic guests. Our results clearly show that the self-filling of the internal cavity of $\text{PrS}[6]^{\text{Et}}$ or $\text{PrS}[6]^{n\text{Pr}}$ stabilizes their D_2 -conformation, controlling the cyclization equilibrium toward their formation. Solid state studies (Figures 1b–c),^[14] showed that four ethyl chains fill about 90% of the inner space of the prism[6]arene.

Concerning the propoxy-derivative $\text{PrS}[6]^{i\text{Pr}}$,^[14] solid state investigations showed that four propyl chains fill the inner cavity in a less effective way (84%). In agreement with the hypothesis of a self-filling template effect, the $\text{PrS}[6]^{\text{Et}}$ is obtained in higher yields (75%) than $\text{PrS}[6]^{n\text{Pr}}$ (65%).^[14] The yield of the hexamer was even lower when 2,6-dibutoxynaphthalene or 2,6-dipentoxynaphthalene was used as starting material, because longer butyl and pentyl chains are less effective to fill the internal cavity of the macrocycle.^[14]

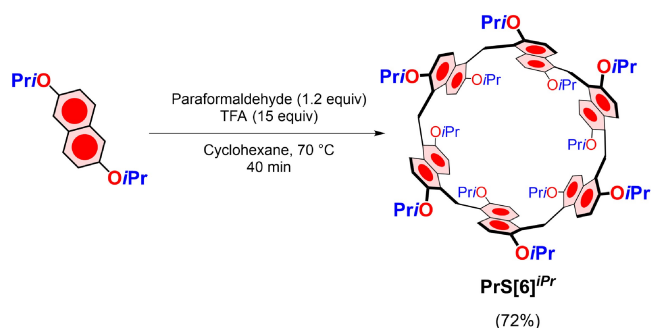
These results indicated clearly that the length of the alkyl chains on the rims of prism[6]arenes play a crucial role to drive their direct macrocyclization.

On the basis of these investigations conducted with linear alkyl substituents, the question arises as to whether the prism[6]arene macrocycle can also be formed and templated by branched alkoxy substituents. In the present manuscript, the direct macrocyclization of 2,6-diisopropoxynaphthalene monomer is described. In addition, the effect of the presence of isopropyl substituents on the molecular recognition features of the naphthalene $\text{PrS}[6]^{i\text{Pr}}$ macrocycle is presented.

Results and Discussion

Synthesis of $\text{PrS}[6]^{i\text{Pr}}$

2,6-Diisopropoxynaphthalene was reacted with paraformaldehyde (1.2 equiv) in cyclohexane (5 mM) at 70 °C for 40 min (Scheme 1), in the presence of trifluoroacetic acid (15 equiv). The reaction was quenched by the addition of NaHCO_3 saturated aqueous solution, and the organic solvent (CH_2Cl_2)



Scheme 1. Synthesis of $\text{PrS}[6]^{i\text{Pr}}$.

was removed under reduced pressure. Finally, the solid residue was washed with ethanol to give $\text{PrS}[6]^{i\text{Pr}}$ as a white solid in 72% yield, which was sufficiently pure without the need for chromatography. Thus, analogously^[14] to $\text{PrS}[6]^{n\text{Pr}}$ and $\text{PrS}[6]^{\text{Et}}$, the isopropoxy-prism[6]arene was obtained in high yields after a short reaction time. With this result in hand we investigated the structure adopted by $\text{PrS}[6]^{i\text{Pr}}$ both in the solid state and in solution.

Structure of $\text{PrS}[6]^{i\text{Pr}}$ in the solid state

The solid state structure of $\text{PrS}[6]^{i\text{Pr}}$ was obtained by single crystal X-ray diffraction (Figure 2 and SI) using synchrotron radiation and cryo-cooling techniques. The asymmetric unit of the centrosymmetric structure (space group = $P2_1/c$) of $\text{PrS}[6]^{i\text{Pr}}$ contains one macrocyclic molecule, 0.90 CH_2Cl_2 molecules statistically distributed across two sites and 0.95 CH_3OH molecules statistically distributed across three sites (see SI for full details). The centrosymmetric crystals therefore contain a racemic mixture of the inherently chiral $\text{PrS}[6]^{i\text{Pr}}$ macrocycles. The highly disordered solvent crystallization molecules are all found in the interstitial spaces of the packing, outside the prismarene macrocycle, which is instead self-filled by the isopropyl arms of the 2,6 diisopropoxynaphthalene subunits (Figure 2).

Analogously to our previously reported structures of $\text{PrS}[6]^R$ ($R = \text{Me}, \text{Et}, n\text{Pr}$),^[14] the $\text{PrS}[6]^{i\text{Pr}}$ macro-ring is folded into a cuboid shape, with the faces defined by the six naphthalene planar groups (Figures 2), and exhibits a dissymmetric conformation with a pseudo- D_2 point symmetry of the macro-ring (Figures 2d,e). The geometric features of the cuboid are comparable to those previously reported (Table S3). Thus, each naphthalene planar moiety makes an interior angle of about 90° with respect to the adjoining naphthalene moieties (Table S3). The two opposite naphthalene rings which define the square faces of the prism (A and A' of Figure 2d) are 11.38 Å apart and show about 90° canting angles (θ) with respect to the mean plane of the methylene bridges, compatible with the pseudo-twofold symmetry axis which passes through the 10-carbon atom centroids of these naphthalene rings (Table S3).

A second orthogonal twofold axis passes through two opposite methylene bridges of naphthalene moieties located on two edges of elongated faces and a third orthogonal twofold axis passes through the two open edges of the prism, to produce a D_2 point symmetry of the cuboid (Figures 2d,e). The naphthalene moieties which define the elongated faces of the cuboid prism show canting angles of ca. 40°/130° for the B/B'' and B'''/B' couples (Figure 2d, Table S3). For a D_2 symmetry the B/B'' and B'''/B' couples should be supplementary angles and the observed difference of about 10° is a measure of the deviation from the ideal point symmetry (Figure 2d). It is worth noting that due to the formation of different C–H ... π interactions within the internal cavities (Figure 2e, Tables S4–S5), there are some conformational differences in the cuboid for the three structures of $\text{PrS}[6]^R$ ($R = i\text{Pr}, \text{Et}, n\text{Pr}$, see Tables S4–S5). Two open edges of the prism in $\text{PrS}[6]^{i\text{Pr}}$ are slightly more open

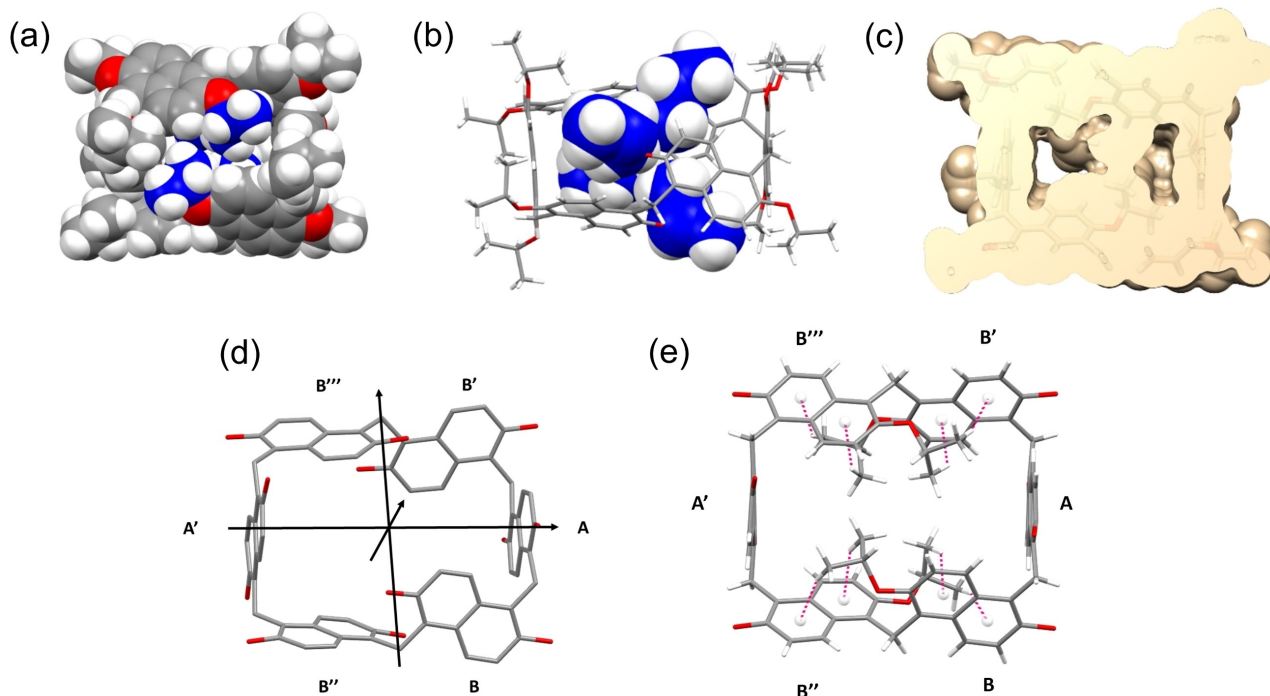


Figure 2. Different views of the self-filling of the cavity of $\text{PrS[6]}^{\text{IPr}}$, as observed in the single crystal X-ray structure, (a) and (b). The isopropyl carbon atoms are in blue. Cross section of the $\text{PrS[6]}^{\text{IPr}}$ molecule (c) evidencing a hole of about 0.65 \AA radius through the cuboid structure. (c) Two enclosed internal cavities were obtained from accessible surface area calculations using a 0.7 \AA probe. The total free cavity volume is 40 \AA^3 . For comparison, using the same probe the free cavity volume values for $\text{PrS[6]}^{\text{Et}}$ and $\text{PrS[6]}^{\text{nPr}}$ are 24 \AA^3 and 60 \AA^3 , respectively.^[14] (d) The pseudo D_2 symmetry of $\text{PrS[6]}^{\text{IPr}}$. (e) C–H $\cdots \pi$ interactions in the cavity of $\text{PrS[6]}^{\text{IPr}}$.

compared to $\text{PrS[6]}^{\text{nPr}}$ and $\text{PrS[6]}^{\text{Et}}$. The deviation from 90° of the interior dihedral angles between adjacent naphthalene planes provides a measure of the deformation of the cuboid structure. Angles larger than 90° indicate an opening of the box, while angles smaller than 90° indicate a more closed box. In this case, the total interior dihedral angles of $\text{PrS[6]}^{\text{IPr}}$ show an opening of the box of more than 23° , whereas $\text{PrS[6]}^{\text{nPr}}$ and $\text{PrS[6]}^{\text{Et}}$ exhibit angles of about 10° and 6° – 8° (two values for the two crystallographically independent molecules), respectively (Table S3).

The four inward-oriented isopropyl groups of the naphthalene moieties located on the elongated faces of the prism (Figure 2e) establish C–H $\cdots \pi$ interactions with the aromatic walls and various inter-chain van der Waals interactions (Figure 2e). Each of these eight methyl groups located in the cavity establishes a C–H $\cdots \pi$ interaction with one phenyl ring of an opposite naphthalene moiety (Figure 2e), for a total of eight strong C–H $\cdots \pi$ interactions. The C–H/ π^{centroid} distance ranges from 2.6 to 3.1 \AA , while the C–H $\cdots \pi^{\text{centroid}}$ angles are in the range 132 – 163° (Table S4). For comparison, in the case of $\text{PrS[6]}^{\text{Et}}$ the interactions involve only four methyl groups, which are positioned above the naphthalene rings to form very asymmetric bifurcated C–H $\cdots \pi$ interactions (Table S5). For $\text{PrS[6]}^{\text{nPr}}$, the total C–H $\cdots \pi$ interactions which involve only four β methylene groups are even weaker (Table S5), while the terminal methyl groups do not interact.

Therefore, on the basis of the C–H $\cdots \pi$ interactions, the $\text{PrS[6]}^{\text{IPr}}$ methyl groups are more strongly held inside the

macrocyclic cavity. On the one hand, these interactions produce a slightly open cuboid with respect to the $\text{PrS[6]}^{\text{Et}}$ and $\text{PrS[6]}^{\text{nPr}}$ analogues, on the other hand the aromatic walls becomes more sticky and the box becomes more difficult to open.

Conformational properties of $\text{PrS[6]}^{\text{IPr}}$ in solution

1D and 2D NMR analysis (Figure 3, and SI) in CD_2Cl_2 is consistent with the D_2 symmetry of the cuboid structure observed in the solid state. The ^1H NMR spectrum of $\text{PrS[6]}^{\text{IPr}}$ in Figure 3 showed the presence of 3 aromatic AX/AB systems (COSY, Figure S3) at $8.24/7.37$ (9.6 Hz), $7.84/6.91$ (9.6 Hz), and $7.53/6.33$ (9.6 Hz) ppm,

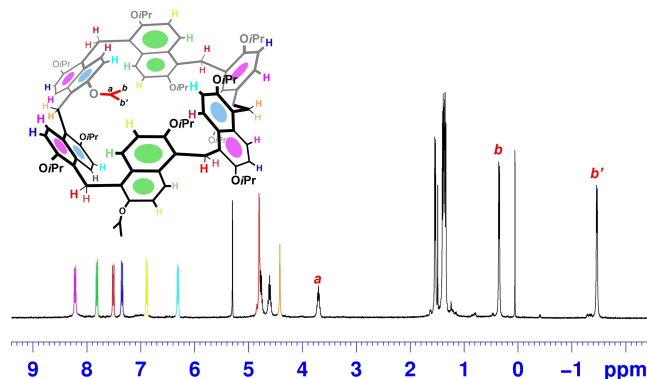


Figure 3. ^1H NMR Spectrum of $\text{PrS[6]}^{\text{IPr}}$ (CD_2Cl_2 , 400 MHz , 298 K).

and two methylene-bridged singlets at 4.83 and 4.44 ppm in a 2:1 ratio. The isopropyl groups give rise to three $\text{OCH}(\text{CH}_3)_2$ multiplets at 3.72, 4.63 and 4.79 ppm in 1/1/1 ratio. The CH multiplet at 4.63 ppm shows a correlation in the 2D COSY spectrum, with a CH_3 -doublet at 1.37 ppm, while two diastereotopic CH_3 -doublets correlate with the CH-multiplet at 4.79 ppm.

Interestingly the $\text{OCH}(\text{CH}_3)_2$ multiplet at 3.72 ppm correlates with two diastereotopic CH_3 -doublets, at 0.38 ppm ($J=6.0$ Hz) and -1.44 ppm ($J=6.0$ Hz), with a large $\Delta\delta$ spacing of 1.82 ppm calculated between these two diastereotopic CH_3 groups. The presence of a shielded CH_3 -doublet at negative value of chemical shift [-1.44 ppm ($J=6.0$ Hz)], clearly confirmed the finding that $\text{PrS}[\mathbf{6}]^{\text{IPr}}$ adopts also in solution the cuboid structure (Figures 2 and 3), in which 4 isopropyl groups are folded inside its cavity. In details, in agreement with the solid state structure of $\text{PrS}[\mathbf{6}]^{\text{IPr}}$ in Figure 2, the doublet at -1.44 ppm is attributable to inward oriented methyl groups (Figures 2 and 3) while the diastereotopic CH_3 -doublet at 0.38 ppm is outward oriented with respect to the $\text{PrS}[\mathbf{6}]^{\text{IPr}}$ cavity. The presence of these diastereotopic resonances for the $\text{OCH}(\text{CH}_3)_2$ groups of $\text{PrS}[\mathbf{6}]^{\text{IPr}}$ is due to the planar chirality of the macrocycle.^[18–22] In fact, the $\text{PrS}[\mathbf{6}]^{\text{IPr}}$ shows six planes of chirality which are coplanar with the 2,6-dialkoxynaphthalene rings and the bridged-methylene carbons at the 1/5 ring positions. In fact, the centrosymmetric crystal structure of $\text{PrS}[\mathbf{6}]^{\text{IPr}}$ is composed of a racemic mixture of chiral macrocyclic molecules, in which naphthalene moieties adopt all-*pS* (or all-*pR*), orientation. ^1H VT NMR experiments in toluene- d_8 (Figure 4a) showed that the

diastereotopic CH_3 -doublets, the aromatic (ArH) and the methylene-bridged (CH_2) signals of the cuboid D_2 -structure of $\text{PrS}[\mathbf{6}]^{\text{IPr}}$ coalesced at 373 K (Figure 4a).^[18,20] These NMR signals coalescences clearly indicate a conformational mobility of the cuboid D_2 -structure of $\text{PrS}[\mathbf{6}]^{\text{IPr}}$ due to the *oxygen-through-the-annulus*^[18,20] passage of the naphthalene units (Figure 4d), which is fast on the NMR time scale at higher temperature (a ΔG^\ddagger value of 18.4 kcal/mol was calculated for this process, see SI). In fact, when a $\text{DMSO}-d_6$ solution of $\text{PrS}[\mathbf{6}]^{\text{IPr}}$ (Figure 4e) was heated at 403 K, then the ^1H NMR spectrum of $\text{PrS}[\mathbf{6}]^{\text{IPr}}$ become more simple and compatible with a more symmetrical $\text{PrS}[\mathbf{6}]^{\text{IPr}}$ structure (see marked signals in Figure 4e).

As previously reported, the ^1H NMR spectrum of $\text{PrS}[\mathbf{6}]^{\text{nPr}}$ at 298 K is also in agreement with a pseudo D_2 point symmetry, and with respect to $\text{PrS}[\mathbf{6}]^{\text{IPr}}$ derivative, a lower coalescence temperature of 323 K (Figure 4b, S8–S9) was found for the NMR signals of the cuboid D_2 -structure of $\text{PrS}[\mathbf{6}]^{\text{nPr}}$, due to the *oxygen-through-the-annulus*^[18,20] passage of the naphthalene units (a ΔG^\ddagger value of 15.2 kcal/mol was calculated). Analogous values were found for $\text{PrS}[\mathbf{6}]^{\text{Et}}$, ^1H VT NMR studies in Figure 4c (Figure S6 and S7), indicate clearly a coalescence at 333 K for the NMR signals of the cuboid D_2 -structure of $\text{PrS}[\mathbf{6}]^{\text{Et}}$ (ΔG^\ddagger value of 15.7 kcal/mol). These results indicated unequivocally that the D_2 -cuboid structure of $\text{PrS}[\mathbf{6}]^{\text{IPr}}$ is conformationally more rigid than the analogous cuboid skeleton of $\text{PrS}[\mathbf{6}]^{\text{nPr}}$ and $\text{PrS}[\mathbf{6}]^{\text{Et}}$. The higher conformational stability of the D_2 -cuboid structure of the isopropoxy-prism[6]arene $\text{PrS}[\mathbf{6}]^{\text{IPr}}$ compared to the propoxy/ethoxy-prism[6]arene can be mainly attributed to the stabilization brought by the isopropyl groups folded inside

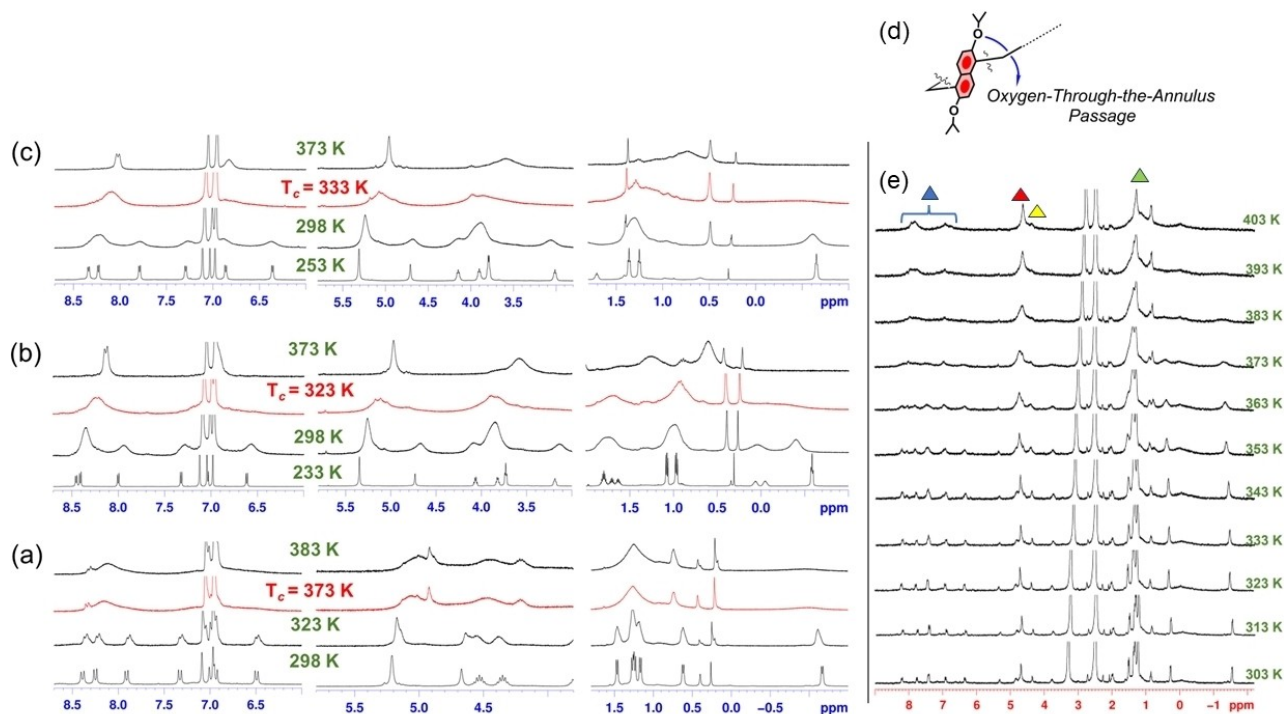


Figure 4. Variable-temperature ^1H NMR spectra: a-c (Toluene- d_8 , 300 MHz) of (a) $\text{PrS}[\mathbf{6}]^{\text{IPr}}$; (b) $\text{PrS}[\mathbf{6}]^{\text{nPr}}$; (c) $\text{PrS}[\mathbf{6}]^{\text{Et}}$. (d) Conformational mobility of $\text{PrS}[\mathbf{6}]^{\text{IPr}}$ due to the *oxygen-through-the-annulus* passage. (e) Variable-temperature ^1H NMR spectra of $\text{PrS}[\mathbf{6}]^{\text{IPr}}$ in $\text{DMSO}-d_6$ (300 MHz): marked in blue, red, yellow and green, the ArH, ArCH_2Ar , $\text{OCH}(\text{CH}_3)_2$ and $\text{OCH}(\text{CH}_3)_2$ signals, respectively.

the cavity of $\text{PrS}[6]^{iPr}$. In agreement with solid state analysis, the methyl groups of the isopropyl chains of $\text{PrS}[6]^{iPr}$, folded inside the cavity of the macrocycle, establish stronger C–H $\cdots\pi$ interactions (Figure 2e) than the methylene groups of the four *endo*-cavity oriented propyl chains of $\text{PrS}[6]^{nPr}$. In other words, C–H $\cdots\pi$ interactions among *endo*-cavity oriented isopropyl groups and the aromatic walls of $\text{PrS}[6]^{iPr}$ are more sticky and generate a sort of conformational friction.

Complexation properties of $\text{PrS}[6]^{iPr}$

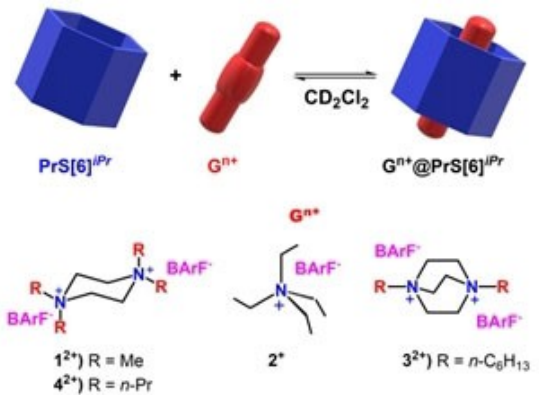
The greater inertia of $\text{PrS}[6]^{iPr}$ to open its cuboid D_2 conformation, with respect to $\text{PrS}[6]^{Et}$ and $\text{PrS}[6]^{nPr}$, also affects its binding abilities. In fact, *isopropoxy*-prism[6]arene forms *endo*-cavity complexes with alkylammonium guests which show lower thermodynamic stability than the analogous complexes of the propoxy/ethoxy-prism[6]arene. An apparent association constant value of $5.2 \times 10^7 \text{ M}^{-1}$ (298 K, CD_2Cl_2) was calculated for the *endo*-cavity complexation of 1^{2+} as BARF^- salt ($1^{2+}@\text{PrS}[6]^{iPr}$ complex, Table 1, ES1†), a value significantly lower than that

calculated for the formation of the $1^{2+}@\text{PrS}[6]^{Et}$ and $1^{2+}@\text{PrS}[6]^{nPr}$ complexes (Table 1, $1.0\text{--}1.2 \times 10^8 \text{ M}^{-1}$).^[14] In detail, the addition of *N,N,N,N'*-tetramethylpiperazonium 1^{2+} (Table 1, Figure 5) as BARF^- salt^[23,24] to a solution of $\text{PrS}[6]^{iPr}$ in CD_2Cl_2 (Figures 5a,b) caused remarkable changes in the ^1H NMR spectrum of $\text{PrS}[6]^{iPr}$ (see Figure 5a and 5b), indicative of the formation of the *endo*-cavity $1^{2+}@\text{PrS}[6]^{iPr}$ complex. In fact, a more symmetric conformation, with an average D_6 symmetry, emerged for the $\text{PrS}[6]^{iPr}$ macrocycle upon *endo*-cavity complexation of 1^{2+} (Figure 5b).

In details, the ^1H NMR signals of 1^{2+} were *up-field* shifted upon its *endo*-cavity inclusion inside the cavity of $\text{PrS}[6]^{iPr}$. The methylene groups of 1^{2+} in the $1^{2+}@\text{PrS}[6]^{iPr}$ complex, were detected at -0.80 ppm and -1.00 ppm (Figure 5b, $J=11.2$ Hz), and experienced a complexation induced shift (C.I.S.; $\Delta\delta = \delta_{\text{complex}} - \delta_{\text{free}}$) of 4.62 ppm with respect to the chemical shift of the free *N,N,N,N'*-tetramethylpiperazonium 1^{2+} as BARF^- salt in CD_2Cl_2 (Figure S11). Diagnostic dipolar couplings were detected in the NOESY spectrum (Figure S14) between host and guest H-atoms, in agreement with the formation of the *endo*-cavity $1^{2+}@\text{PrS}[6]^{iPr}$ complex. In addition, diagnostic couplings were detected between shielded methylene signals of 1^{2+} at $-0.80/-1.00$ ppm, and *ArH* signals of $\text{PrS}[6]^{iPr}$ at 8.88 and 7.18 ppm (Figure S14).

A naphthalene aromatic AX system was detected at 8.88 and 7.18 ppm with a $\Delta\delta = 1.70$ ppm, while an ArCH_2Ar singlet was present at 4.78 ppm (Figure 5b). Concerning the isopropyl resonances, the $1^{2+}@\text{PrS}[6]^{iPr}$ complex showed a $\text{OCH}(\text{CH}_3)_2$ multiplet at 4.68 ppm and two diastereotopic $\text{OCH}(\text{CH}_3)_2$ doublets at 1.57 and 1.28 ppm. Finally, these results confirm that 1^{2+} occupied the internal cavity of $\text{PrS}[6]^{iPr}$, and forced the cuboid scaffold to open (Figure 6) in a more symmetrical D_6 -structure. DFT-optimized structure of the $1^{2+}@\text{PrS}[6]^{iPr}$ complex at the B97D3/SVP/SVPFIT level of theory, (Figure 6b) has been performed. The cation 1^{2+} takes on an orientation in which the average plane of the cyclohexane ring is tilted by 20° with respect to the mean plane of the $\text{PrS}[6]^{iPr}$ methylene-bridged groups. In this geometry, the methylene H-atoms of the guest point to the aromatic cavity of $\text{PrS}[6]^{iPr}$, to give C–H $\cdots\pi$

Table 1. Association constant (K_{ass} , M^{-1} , CD_2Cl_2 , 298 K) values for the formation of the complexes between the ammonium 1^{2+} – 4^{2+} cations as BARF^- salts and $\text{PrS}[6]^{iPr}$, $\text{PrS}[6]^{nPr}$, $\text{PrS}[6]^{Et}$ prism[6]arenes.



	$\text{Pr}[6]^{iPr}$	$\text{Pr}[6]^{nPr}$	$\text{Pr}[6]^{Et}$
1^{2+}	$5.2 \pm 0.9 \times 10^7$ [a]	$1.2 \pm 0.2 \times 10^8$ [a]	$1.0 \pm 0.2 \times 10^8$ [a]
2^+	No complex	340 ± 50 [a]	$2.7 \pm 0.4 \times 10^3$ [a]
3^{2+}	60 ± 9 [a]	400 ± 60 [a]	790 ± 100 [a]
4^{2+}	890 ± 100 [a]	$1.4 \pm 0.2 \times 10^3$ [a]	$1.3 \pm 0.2 \times 10^3$ [a]

[a] The binding constant was calculated by ^1H NMR competition experiments. [b] The binding constant was calculated by integration of ^1H NMR signals of free and complexed host. [c] Reference [14].

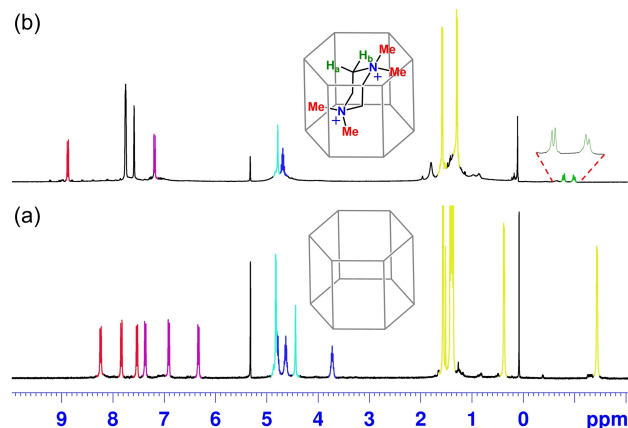


Figure 5. (a and b) ^1H NMR spectra of $\text{PrS}[6]^{iPr}$ (a) in CD_2Cl_2 at 298 K (400 MHz) and (b) a 1:1 mixture of $\text{PrS}[6]^{iPr}$ and 1^{2+} as barfate salt (3.9 mM).

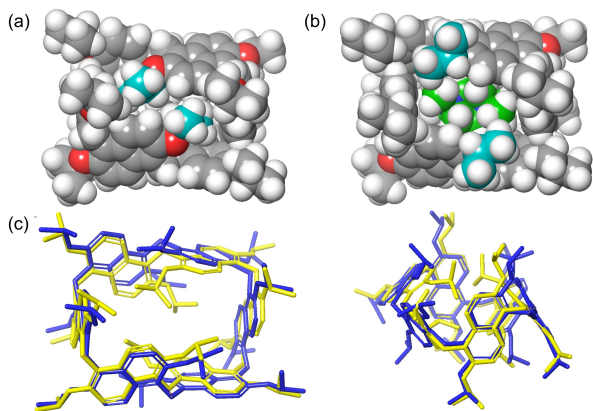


Figure 6. (a) DFT-optimized structure of the D_2 -cuboid structure of $\text{Pr}[6]^{iPr}$ (closed state). (b) DFT-optimized structure of the $1^{2+}@Pr[6]^{iPr}$ complex. (c) Superimposition of the DFT-optimized structures of $\text{Pr}[6]^{iPr}$ (closed state; yellow) and complexed $\text{Pr}[6]^{iPr}$ form (open state; blue), the guest 1^{2+} is omitted for clarity.

interactions with an average $\text{C}-\text{H}\cdots\pi_{\text{centroid}}$ distance of 2.51 \AA (Figure S25). The *endo*-cavity complexation of 1^{2+} , moving from a closed to an open state of the macroring, pushed the isopropyl groups out from the cavity as highlighted in Figure 6c. Similar conformational changes, from a closed to an open conformation (Figure 6), were also observed by NMR upon *endo*-cavity complexation of 3^{2+} and 4^{2+} inside the cavity of $\text{PrS}[6]^{iPr}$ (Figure 7). In particular, upon formation of the $3^{2+}@Pr[6]^{iPr}$ complex in CD_2Cl_2 at 298 K (Figure 7b), the host adopted the D_6 -symmetrical conformation as confirmed by the ^1H NMR spectrum of the mixture. An aromatic AX system was detected at 8.33 and 7.08 ppm with a $\Delta\delta = 1.25$ ppm, attributable to the naphthalene H-atoms of $\text{PrS}[6]^{iPr}$ (Figure 7b). A sharp singlet at 4.79 is attributable to the bridged methylene groups,

while the $\text{CH}(\text{CH}_3)_2$ H-atoms resonate as a multiplet at 4.64 ppm. Finally, two doublets were present at 1.55 and 1.32 ppm, attributable to the diastereotopic methyl groups of the isopropyl chains. An association constant value of 60 M^{-1} (Table 1) was calculated by direct integration of slowly exchanging ^1H NMR signals of the $3^{2+}@Pr[6]^{iPr}$ complex and the free host (Figure 7b). This value is significantly lower than those previously reported for the formation of $3^{2+}@Pr[6]^{nPr}$ and $3^{2+}@Pr[6]^{Et}$ complexes of 400 and 790 M^{-1} , respectively (Table 1).^[14]

In a previous work,^[14] we reported an association constant value of 340 M^{-1} for the formation of the $2^{+}@Pr[6]^{iPr}$ complex, while in the presence of $\text{PrS}[6]^{iPr}$ no evidence of complexation of 2^{+} was observed in the experimental condition used (SI). Finally, the formation of the $4^{2+}@Pr[6]^{iPr}$ complex in CD_2Cl_2 shows ^1H NMR spectral features (Figure 7c) similar to those discussed above, with the typical signature at high-field negative values of chemical shift and the emergence of the aromatic AX system (8.82 and 7.13 ppm). By direct integration of the slowly exchanging ^1H NMR signals of the $4^{2+}@Pr[6]^{iPr}$ complex and the free host (ESI), an association constant value of 890 M^{-1} was calculated (Table 1). Again, this value is lower than those observed for the formation of $4^{2+}@Pr[6]^{nPr}$ and $4^{2+}@Pr[6]^{Et}$ complexes of 1.4×10^3 and $1.3 \times 10^3 \text{ M}^{-1}$, respectively (Table 1).

Conclusions

The direct macrocyclization of isopropoxyprism[6]arene $\text{PrS}[6]^{iPr}$ bearing branched isopropyl chains on the rims is here described. Analogously to propoxy- and ethoxy-prism[6]arene, $\text{PrS}[6]^{iPr}$ also adopts a cuboid D_2 -conformation, both in solution and in the solid state. The D_2 -structure of $\text{PrS}[6]^{iPr}$ shows four

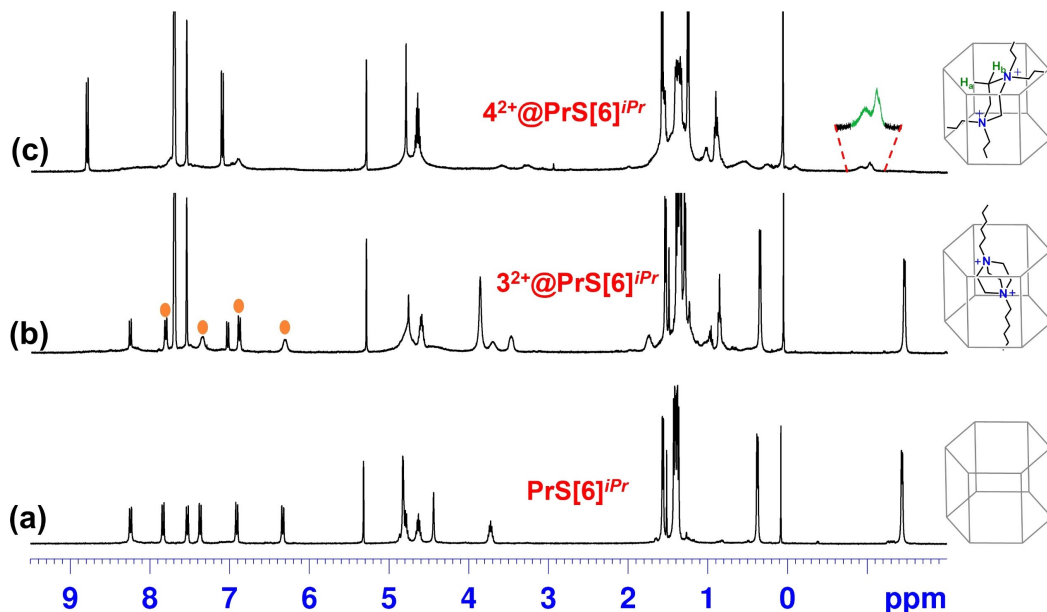


Figure 7. ^1H NMR spectra (CD_2Cl_2 , 400 MHz, 298 K) of (a) $\text{Pr}[6]^{iPr}$, (b) a 1 : 1 mixture of $\text{Pr}[6]^{iPr}$ and $3^{2+} \cdot (\text{BArF})_2$ (3.9 mM), (c) a 1 : 1 mixture of $\text{Pr}[6]^{iPr}$ and $4^{2+} \cdot (\text{BArF})_2$ (3.9 mM). In Figure 7b, marked with an orange dot the signals of the free $\text{Pr}[6]^{iPr}$ host.

isopropyl groups folded inside the cavity, to give C–H... π interactions and self-filling of the internal space. The conformational features of isopropoxyprism[6]arene were studied by ^1H VT NMR investigations. By these studies, it is clear that the D_2 -cuboid structure of $\text{PrS}[6]^{iPr}$ is conformationally more rigid than the analogous ethoxy and propoxy-hexamers. Thus, the presence of branched isopropyl chains on the prism[6]arene rims, stabilizes the cuboid D_2 -conformation of $\text{PrS}[6]^{iPr}$ to a greater extent than ethyl or propyl groups in $\text{PrS}[6]^{Et}$ and $\text{PrS}[6]^{nPr}$.

The greater inertia of $\text{PrS}[6]^{iPr}$ to open its cuboid D_2 conformation is due to a peculiar "conformational friction" created by isopropyl groups on the rims of the macrocycle, by their cavity-filling effects and secondary C–H... π interactions. As a result, alkylammonium-based *endo*-cavity complexes of $\text{PrS}[6]^{iPr}$ show lower binding constants values than the analogous propoxy/ethoxy-prism[6]arene complexes.

Experimental Section

General: HR MALDI mass spectra were recorded on a Bruker Solarix FT-ICR mass spectrometer equipped with a 7T magnet. The samples recorded in MALDI were prepared by mixing 10 μL of analyte in dichloromethane (1 mg/mL) with 10 μL of solution of 2,5-dihydroxybenzoic acid (10 mg/mL in Methanol). The mass spectra were calibrated externally, and a linear calibration was applied. All chemical reagents grade was used without further purification and were used as purchased by Merck, TCI and Fluorochem. Reaction temperatures were measured externally. Reactions were monitored by Merck TLC silica gel plates (0.25 mm) and visualized by UV light 254 nm. NMR spectra were recorded on a Bruker Avance-600 [600 (^1H)], Avance-400 [400 (^1H) and 100 MHz (^{13}C)] and Avance-300 [300 (^1H) and 75 MHz (^{13}C)] spectrometers. Chemical shifts are reported relative to the residual solvent peak.²⁵ Standard pulse programs, provided by the manufacturer, were used for 2D COSY (cosygpqf), 2D HSQC (hsqcetdgpisp2.2) and 2D NOESY (noesygpqppp) experiments. Structural assignments were made with additional information from gCOSY, gHSQC, and geNOESY experiments.

Synthesis of $\text{PrS}[6]^{iPr}$: A solution of 2,6-diisopropoxynaphthalene (500 mg, 2.05 mmol), paraformaldehyde (74 mg, 2.45 mmol, 1.2 equiv) in 400 mL of cyclohexane (5 mM) was heated to 70 $^\circ\text{C}$, then trifluoroacetic acid (2.3 mL, 0.03 mol, 15 equiv) was added. The solution was stirred for 40 min at 70 $^\circ\text{C}$, then an aqueous saturated solution of NaHCO_3 (100 mL) was poured in the reaction mixture and the organic layer was extracted. The aqueous layer was washed with CH_2Cl_2 (2 \times 50 mL) and the organic phases were collected and dried over Na_2SO_4 . The solvent was removed under reduced pressure, and then the solid residue was washed several times with ethanol (3 \times 50 mL) to give derivative $\text{PrS}[6]^{iPr}$ as a white solid (380 mg, 72%).

Derivative $\text{PrS}[6]^{iPr}$: M.p.: >310 $^\circ\text{C}$ dec. ^1H NMR (400 MHz, CD_2Cl_2 , 298 K): δ = 8.24 (*d*, J = 9.6 Hz, ArH, 4H), 7.84 (*d*, J = 9.6 Hz, ArH, 4H), 7.53 (*d*, J = 9.6 Hz, ArH, 4H), 7.37 (*d*, J = 9.6 Hz, ArH, 4H), 6.91 (*d*, J = 9.6 Hz, ArH, 4H), 6.33 (*d*, J = 9.6 Hz, ArH, 4H), 4.83 (*overlapped*, ArCH₂Ar, 8H), 4.79 (*m*, –OCH, 4H), 4.63 (*m*, –OCH, 4H), 4.44 (*s*, ArCH₂Ar, 4H), 3.72 (*m*, –OCH, 4H), 1.56 (*d*, J = 6.0 Hz, –CHCH₃, 12H), 1.42 (*d*, J = 6.0 Hz, –CHCH₃, 12H), 1.39 (*d*, J = 6.0 Hz, –CHCH₃, 12H), 1.37 (*d*, J = 6.0 Hz, –CHCH₃, 12H), 0.38 (*d*, J = 6.0 Hz, –CHCH₃, 12H), –1.44 (*d*, J = 6.0 Hz, –CHCH₃, 12H). ^{13}C NMR { ^1H } (75 MHz, CD_2Cl_2 , 298 K): δ = 151.3, 150.3, 131.0, 130.5, 129.4, 126.6, 125.8, 125.4, 125.1, 124.6, 123.9, 116.9, 115.7, 114.1, 72.3, 71.6, 68.9, 23.2, 22.9,

22.7, 22.4, 19.1. HRMS (MALDI): m/z calcd for $\text{C}_{102}\text{H}_{120}\text{O}_{12}$: 1536.8780; found 1536.8772.

^1H NMR determination of K_{ass} values: The association constant values of complexes were calculated by means of two methods:

- ^1H NMR competition experiments. In this case, we performed an analysis of a 1:1:1 mixture of guest, and two hosts in an NMR tube by using 0.5 mL of CD_2Cl_2 as solvent.
- Integration of ^1H NMR signals of free and complexed host. In this case, an equimolar solution of hosts and guests was solubilized in CD_2Cl_2 and equilibrated in a NMR tube after mixing for 24–96 h at 40 $^\circ\text{C}$, to favour kinetically the complexation.

All K_{ass} values were calculated at 298 K (no substantial difference was observed by calculating the constant at 338 K), and ^1H NMR experiments were recorded on 400 MHz spectrometers. Errors < 15% were calculated as mean values of three measures.

DFT Calculations: DFT-optimized structures have been performed using the DFT method incorporated in the Gaussian 16^[26] package and using B97D3/SVP/SVPFIT level of theory. The starting structure for DFT calculations were obtained by Monte Carlo simulated annealing procedure. All optimized structures were characterized by 0 imaginary frequency.

Crystallographic structure of $\text{PrS}[6]^{iPr}$: Colourless single crystals were obtained by slow evaporation of solutions of $\text{PrS}[6]^{iPr}$, using a mixture of CH_2Cl_2 and CH_3OH as solvent. Data collection was carried out at the XRD1 beamline of the Elettra synchrotron (Trieste, Italy) using the rotating-crystal method, with a monochromatic wavelength of 0.7000 \AA and a Dectris Pilatus 2 M area detector. Single crystals were dipped in paratone cryoprotectant, mounted on a nylon loop and flash-frozen under a nitrogen stream at 100 K. Diffraction data were indexed and integrated using the XDS package,^[27] while scaling was carried out with XSCALE.^[28] The structure was solved using the SHELXT^[29] program and structure refinement was performed with SHELXL-18^[30,31] by full-matrix least-squares (FMLS) methods on F^2 , operating through the WinGX GUI.^[32] Non-hydrogen atoms of the prism[n]arene macrocycles were refined anisotropically, except for carbon and oxygen atoms with occupancy factor less than 0.5 (see SI). Hydrogen atoms were included in idealised positions and refined using the riding model. Crystallographic data and refinement details are reported in Table S2.

Deposition Number 2251127 ($\text{PrS}[6]^{iPr}$) contains the supplementary crystallographic data for this paper. These data are provided free of charge by the joint Cambridge Crystallographic Data Centre and Fachinformationszentrum Karlsruhe Access Structures service.

Supporting Information

Electronic supplementary information (ESI) available. 1D and 2D NMR spectra of prismarenes and their complexes, HR mass spectra, details on stability constant determination, DFT calculation details. X-ray Figures, and table of crystal data.

Conflict of Interests

The authors declare no conflict of interest.

Data Availability Statement

The data that support the findings of this study are available in the supplementary material of this article.

Keywords: cavity self-filling effects · supramolecular chemistry · macrocycles · molecular recognition · prismarenes

- [1] C. Gaeta, D.-X. Wang, *Front. Chem.* **2020**, *8*, 128.
- [2] H. Yao, W. Jiang, *Naphthol-Based Macrocycles* (Eds.: Y. Liu, Y. Chen, H. Y. Zhang), Handbook of Macrocyclic Supramolecular Assembly, Springer, Singapore, **2019**.
- [3] J. M. Benyus, *Biomimicry: Innovation Inspired by Nature*, Harper Perennial, **2002**.
- [4] F. Jia, Z. He, L.-P. Yang, Z.-S. Pan, M. Yi, R.-W. Jiang, W. Jiang, *Chem. Sci.* **2015**, *6*, 6731–6738.
- [5] L.-P. Yang, X. Wang, H. Yao, W. Jiang, *Acc. Chem. Res.* **2020**, *53*, 198–208.
- [6] X.-N. Han, Y. Han, C.-F. Chen, *J. Am. Chem. Soc.* **2020**, *142*, 8262–8269.
- [7] R. Del Regno, P. Della Sala, A. Spinella, C. Talotta, D. Iannone, S. Geremia, N. Hickey, P. Neri, C. Gaeta, *Org. Lett.* **2020**, *22*, 6166–6170.
- [8] a) F. Jia, H. Hupatz, L.-P. Yang, H. V. Schröder, D.-H. Li, S. Xin, D. Lentz, F. Witte, X. Xie, B. Paulus, C. A. Schalley, W. Jiang, *J. Am. Chem. Soc.* **2019**, *141*, 4468–4473; b) F. Jia, H. V. Schröder, L.-P. Yang, C. von Essen, S. Sobottka, B. Sarkar, K. Rissanen, W. Jiang, C. A. Schalley, *J. Am. Chem. Soc.* **2020**, *142*, 3306–3310.
- [9] X. Wang, F. Jia, L.-P. Yang, H. Zhou, W. Jiang, *Chem. Soc. Rev.* **2020**, *49*, 4176–4188.
- [10] H. Yao, H. Ke, X. Zhang, S.-J. Pan, M.-S. Li, L.-P. Yang, G. Schreckenbach, W. Jiang, *J. Am. Chem. Soc.* **2018**, *140*, 13466–13477.
- [11] a) F. Jia, H. V. Schröder, L.-P. Yang, C. von Essen, S. Sobottka, B. Sarkar, K. Rissanen, W. Jiang, C. A. Schalley, *J. Am. Chem. Soc.* **2020**, *142*, 3306–3310; b) X.-N. Han, Y. Han, C.-F. Chen, *J. Am. Chem. Soc.* **2020**, *142*, 8262–8269.
- [12] P. Della Sala, R. Del Regno, C. Talotta, A. Capobianco, N. Hickey, S. Geremia, M. De Rosa, A. Spinella, A. Soriente, P. Neri, C. Gaeta, *J. Am. Chem. Soc.* **2020**, *142*, 1752–1756.
- [13] L.-P. Yang, W. Jiang, *Angew. Chem. Int. Ed.* **2020**, *7*, 15794–15796.
- [14] P. Della Sala, R. Del Regno, L. Di Marino, C. Calabrese, C. Palo, C. Talotta, S. Geremia, N. Hickey, A. Capobianco, P. Neri, C. Gaeta, *Chem. Sci.* **2021**, *12*, 9952–9961.
- [15] R. Del Regno, P. Della Sala, D. Picariello, C. Talotta, A. Spinella, P. Neri, C. Gaeta, *Org. Lett.* **2021**, *23*, 8143–8146.
- [16] R. Del Regno, G. D. G. Santonoceta, P. Della Sala, M. De Rosa, A. Soriente, C. Talotta, A. Spinella, P. Neri, C. Sgarlata, C. Gaeta, *Org. Lett.* **2022**, *24*, 2711–2715.
- [17] P. Della Sala, R. Del Regno, A. Capobianco, V. Iuliano, C. Talotta, S. Geremia, N. Hickey, P. Neri, C. Gaeta, *Chem. Eur. J.* **2023**, *29*, e202203030.
- [18] T. Ogoshi, K. Masaki, R. Shiga, K. Kitajima, T.-A. Yamagishi, *Org. Lett.* **2011**, *13*, 1264–1266.
- [19] N. L. Strutt, H. Zhang, J. F. Stoddart, *Chem. Commun.* **2014**, *50*, 7455–7458.
- [20] T. Ogoshi, K. Kitajima, T. Aoki, S. Fujinami, T.a. Yamagishi, Y. Nakamoto, *J. Org. Chem.* **2010**, *75*, 3268–3273.
- [21] K. Wada, M. Suzuki, T. Kakuta, T.-a. Yamagishi, S. Ohtani, S. Fa, K. Kato, S. Akine, T. Ogoshi, *Angew. Chem. Int. Ed.* **2023**, *62*, e202217971.
- [22] K. Adachi, S. Fa, K. Wada, K. Kato, S. Ohtani, Y. Nagata, S. Akine, T. Ogoshi, *J. Am. Chem. Soc.* **2023**, *145*, 8114–8121.
- [23] C. Gaeta, C. Talotta, F. Farina, G. Campi, M. Camalli, P. Neri, *Chem. Eur. J.* **2012**, *18*, 1219–1230.
- [24] C. Gaeta, C. Talotta, P. Neri, *Chem. Commun.* **2014**, *50*, 9917–9920.
- [25] G. R. Fulmer, A. J. M. Miller, N. H. Sherden, H. E. Gottlieb, A. Nudelman, B. M. Stoltz, J. E. Bercaw, K. I. Goldberg, *Organometallics* **2010**, *29*, 2176–2179.
- [26] Gaussian 16, Revision C.01, M. J. Frisch, G. W. Trucks, H. B. Schlegel, G. E. Scuseria, M. A. Robb, J. R. Cheeseman, G. Scalmani, V. Barone, G. A. Petersson, H. Nakatsuji, X. Li, M. Caricato, A. V. Marenich, J. Bloino, B. G. Janesko, R. Gomperts, B. Mennucci, H. P. Hratchian, J. V. Ortiz, A. F. Izmaylov, J. L. Sonnenberg, D. Williams-Young, F. Ding, F. Lipparini, F. Egidi, J. Goings, B. Peng, A. Petrone, T. Henderson, D. Ranasinghe, V. G. Zakrzewski, J. Gao, N. Rega, G. Zheng, W. Liang, M. Hada, M. Ehara, K. Toyota, R. Fukuda, J. Hasegawa, M. Ishida, T. Nakajima, Y. Honda, O. Kitao, H. Nakai, T. Vreven, K. Throssell, J. A. Montgomery, Jr., J. E. Peralta, F. Ogliaro, M. J. Bearpark, J. J. Heyd, E. N. Brothers, K. N. Kudin, V. N. Staroverov, T. A. Keith, R. Kobayashi, J. Normand, K. Raghavachari, A. P. Rendell, J. C. Burant, S. S. Iyengar, J. Tomasi, M. Cossi, J. M. Millam, M. Klene, C. Adamo, R. Cammi, J. W. Ochterski, R. L. Martin, K. Morokuma, O. Farkas, J. B. Foresman, D. J. Fox, Gaussian, Inc., Wallingford CT, **2019**.
- [27] W. Kabsch, *Acta Crystallogr. Sect. D* **2010**, *66*, 125–132.
- [28] W. Kabsch, *Acta Crystallogr. Sect. D* **2010**, *66*, 133–144.
- [29] G. M. Sheldrick, *Acta Crystallogr. Sect. A* **2015**, *71*, 3–8.
- [30] G. M. Sheldrick, *Acta Crystallogr.* **2015**, *C71*, 3–8.
- [31] L. J. Farrugia, *J. Appl. Crystallogr.* **2012**, *45*, 849–854.